Received January 8, 2020, accepted January 17, 2020, date of publication January 21, 2020, date of current version January 29, 2020.

Digital Object Identifier 10.1109/ACCESS.2020.2968352

Data Driven Modeling of the Reactive Oxygen Species Stimulated by Photon Energy in Light Therapies

JIANFEI DONG[1] AND TIANFENG WANG[1,2]

[1]Suzhou Institute of Biomedical Engineering and Technology, Chinese Academy of Sciences, Suzhou 215123, China
[2]Department of Microelectronics, Delft University of Technology, 2628 Delft, The Netherlands

Corresponding author: Jianfei Dong (jfeidong@hotmail.com)

This work was supported in part by the National Natural Science Foundation of China under Grant 61873263, in part by the National Key Research and Development Program of China under Grant 2017YFC0108502, and in part by the Nanjing Institute of Intelligent Health and Innovation, Nanjing Branch of SIBET, under Grant Y85K023705.

ABSTRACT Light therapies can be used to treat fungal infections. A general mechanism is attributed to the generation of cytotoxic reactive oxygen species (ROS) due to light stimulation. The effectiveness of these therapies has been widely studied in the literature via conducting biological experiments, where fungi are exposed to light with various wavelengths and power. However, despite the large amount of work reporting the experimental results, few efforts have been given to build a mathematical model that describes the amount of generated ROS as a function of the photon energy and power of the stimulating light. The lack of such a model still hinders the optimization of the light doses. In this work, we propose a novel modeling method based on experimental data, so as to establish a mathematical relationship between the ROS concentration and the stimulating photon energy and light fluence (energy density). The anti-fungal experiments were performed on *Candida albicans* (*C. albicans*) using four LED light sources with different wavelengths ranging from 385nm to 450nm. Both the viability of the fungi and the ROS concentration therein were measured during the experiments. High fitting accuracy has been achieved by the model, which therefore demonstrates the effectiveness of the proposed modeling techniques.

INDEX TERMS Biomedical engineering, data driven modeling, light-emitting diodes, light therapy, parameter estimation.

I. INTRODUCTION

Light therapies can kill fungi and hence treat fungal infections. One of the major infectious types of fungi is *C. albicans* [1], which is widely found in nature, and commonly occurs as a superficial infection on mucous membranes, e.g. in mouths [2], vaginas [3] and intestines [4]. The treatment of fungal infections by light is a non-antibiotic approach, and can avoid many side effects of antibiotic treatments, e.g. drug resistance [5].

Various blue light within the range of 400–470nm has been studied for anti-fungal therapies. The range with the most effective anti-fungal effect has been found in various studies to be 402–420nm [6]. For instance, 405nm light was proven to be highly effective against the pre-germinated spores of eight different types of fungi [7]. Besides, 415nm blue light was successfully applied to eliminate *C. albicans* in both in vitro and in vivo experiments [8].

The underlying mechanism of the anti-fungal effect of light has not yet been fully understood. A widely accepted hypothesis is that the photons from blue light can excite endogenous intracellular photosensitizers (PS), which in turn produces highly toxic ROS to cells [6], such as singlet oxygen ($^1O_2$), hydroxyl radials ($HO^\bullet$) and etc. Modeling the amount of generated ROS is hence an important issue in order to design the doses, e.g. the photon energy and light power, for an optimal effect in these therapies. However, developing such a mathematical model is a challenging task. The reason can be attributed to the complexities in the photosensitized oxidation reactions, in which the exact types of reactions that take place in the fungi and the exact types of ROS that are generated are actually uncertain [9].

ROS modeling has also been reported as an important problem, and studied in other therapies. For instance, modeling the

The associate editor coordinating the review of this manuscript and approving it for publication was Henry Hess.

ROS density in the plasma generated by dielectric barrier discharge has recently been reported in [10], which can be used in wound healing and dermatological therapies. Moreover, in photodynamic therapies (PDTs), i.e. the light therapies that apply exogenous PS, modeling the dynamic changes in ROS concentration has been well studied, e.g. [11]–[13]. For instance, a set of coupled differential equations are used to describe a PDT process, including seven Michaelis-Menten type equations [14] describing the dynamic changes in the concentrations of respectively the ground, singlet and triplet state of PS, the singlet and triplet state of oxygen, superoxide anions ($O_2^{-\bullet}$), and finally the ROS acceptors excluding the photosensitizer molecules [13]. Moreover, Monte Carlo simulations have been combined with these kinds of kinetic models, and proven to be an effective method for simulating light transport in biological tissues [15], [16]. Nevertheless, the aforementioned kinetic models demonstrate high nonlinearity, and moreover contain many different unknown parameters related to the PS characteristics that shall be determined from dedicated experiments. For instance, up to 21 parameters are required to describe the process of using some FDA or EMA approved PS [13].

Although anti-fungal light therapies are also believed to be caused by the PS that naturally exist in fungal cells, due to the aforementioned uncertain mechanisms of these processes (i.e. what types of reactions and produced ROS), modeling by the first principles becomes even more challenging than modeling a PDT process. To deal with these modeling challenges, a data-driven modeling approach is proposed in this work, which builds the functional relationship between the ROS concentration and two important parameters of the stimulating light, i.e. its photon energy and fluence, by fitting a parameterized model from experimental data. The model structure is motivated from the trend of the time sequence of $^1O_2$ concentrations at a time scale longer than one minute as shown in [12], which is monotonically increasing in a fashion similar to the step response of a first order linear dynamic system [17]. Then, the reaction rate constant in this model is fitted to the photon energy of four different light wavelengths of 385nm, 405nm, 415nm and 450nm. It is also worth mentioning here that the complicated nonlinear dynamics of the first-principle PDT models mainly occur at a tiny time scale, i.e. below one second [12]. Fortunately, this transient behaviour is not of key importance for quantifying the long-term ROS accumulation in light therapies. In fact, many other studies have reported similar gradually increasing ROS accumulations in cells by light stimulation in a time duration of up to hundreds of minutes, e.g. [18], [19].

The contributions of this work are four folds. Firstly, the anti-fungal experiments on *C. albicans* were conducted using four LED light sources with four different wavelengths, including 385nm, 405nm, 415nm and 450nm. Both the viability of the fungi and the ROS concentrations were measured during the experiments. Secondly, a first order linear dynamic model is parameterized for the ROS variations, whose parameters were then estimated from the experimental data. Thirdly, the functional relationship between the reaction rate constants in the four fitted models respectively of 385nm, 405nm, 415nm and 450nm and their corresponding photon energy were constructed. Finally, a complete mathematical model of the ROS concentration induced by light irradiation is established, taking as variables the photon energy and fluence of the light. To the best of our knowledge, it is the first attempt to build such a mathematical model to mathematically describe the induced ROS in vitro without utilizing any exogenous PS. The main symbols used throughout the paper are defined in Table 1.

TABLE 1. Main parameters used in the model.

Quantity	*Unit*	*Symbol*
irradiance	mW/cm^2	E_e
fluence	J/cm^2	H_e
photon energy	eV	E_p
wavelength	nm	λ
ROS concentration	μM	y
reaction rate	none	k

TABLE 2. Applied LEDs and their main parameters, where "W.L." stands for wavelength.

Specified Peak W.L. (nm)	*Type*	*Measured Peak W.L. (nm)*	*Photon Energy (eV)*
385nm	Vishay VLMU3500-385-120	386.2	3.21
405nm	Kingbright ATDS3534UV405B	400.9	3.09
415nm	LUMILEDS LUXEON LHUV-0415-A070	416.5	2.98
450nm	Cree XLampXPE2	447.6	2.77

II. MATERIALS AND METHODS

A. LED LIGHT SOURCE DESIGN

Four different types of LEDs with the specified peak wavelengths respectively at 385nm, 405nm, 415nm and 450nm were applied in this work. The types of these LEDs and their main parameters are listed in Table 2. Their spectral power density (SPD) curves, as measured by a Maya2000Pro spectrometer (Ocean Optics, US), are depicted in Fig. 1(a). In this figure, every SPD curve is normalized with respect to its integral over the range of the measured wavelength, i.e. with each normalized SPD curve integrating to 1.

The LED light sources were designed following the procedures in [20], and were driven by a constant current source with PWM current level control to stabilize the output irradiance [21], [22]. The LED chips are arranged in either a 1.5cm-by-1.5cm square as a 4-by-4 array (385nm, 405nm and 415nm) or a 1cm-by-1cm square as a 3-by-3 array (450nm). The four LED light sources can deliver an irradiance of $50mW/cm^2$ uniformly within a $60cm$-diameter circle. Fig. 1(c) shows the simulated irradiance distribution, where the average irradiance in the 6cm-diameter circle is $49.39mW/cm^2$, with a relative variation of only 6.56%. The irradiance was measured and confirmed by a PM100D power meter with a S120VC probe (Thorlabs, Newton, NJ, US).

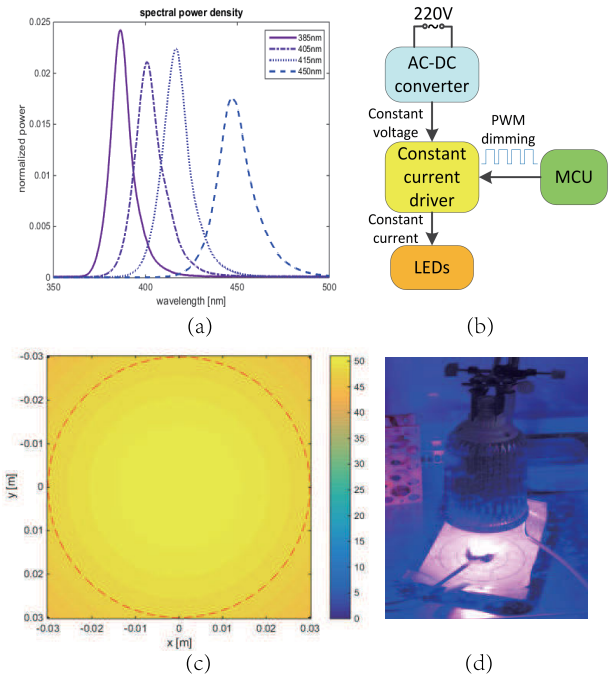

FIGURE 1. LED light source design: (a) normalized SPD of the four types of LEDs, (b) electrical scheme, (c) simulated irradiance distribution, (d) photo of the experimental setup.

The schematic diagram of the electrical drive and control system and the experimental setup are illustrated in Figs. 1(b) and 1(d).

B. EXPERIMENTAL METHODS

1) ANTI-FUNGAL ASSAY

The *C. albicans* strain used in this work is the 3147 (IFO 1594) strain (ATCC, US). The fungal viability was estimated by colony counting in terms of colony-forming units (CFU). After the concentration of the fungi reached 10^7cells/ml, the fungal suspension was diluted by 10^4-fold with sterilized water. The diluted suspension was then spread on tryptic soy agar (TSA), and divided into a control group and a treatment group. The treatment group was respectively irradiated by one of the four LED light sources; while the control group was kept in the dark. The distances from the light sources to the fungi were around 10cm in all the cases to achieve the target irradiance of $50mW/cm^2$.

More specifically, the light irradiation experiments were performed at each sampling instant of respectively 0, 5, 10, 15, 20, 25 and 30 minutes under the 385nm, 405nm and 415nm light exposure; and at 0, 15, 30, 45, 60, 75, 90, 105 and 120 minutes under the 450nm light irradiation, because it takes longer time for this wavelength to achieve a significant fungal inhibition at the same irradiance. At each of these sampling instants, one agar plate spread with the fungal suspension was exposed to the light; and another plate spread with the same suspension was kept in the dark. Moreover, only one plate was exposed to the light at each light irradiation experiment. Therefore, three plates were separately irradiated by the light at different time for each sampling instant. Afterwards, all the six plates were cultured for 24-48 hours at 26^oC, before the colony counting. These steps resulted in triplicate experiments for each treatment time interval, whose raw CFU data were then processed to produce the mean and standard deviation of the viability rates at each sampling instant. The significance of the growth inhibition of the fungi before and after the light treatment was tested by the Student's t-test.

2) ROS ASSAY

For the homogeneity of the ROS measurements, the concentrations of the fungi used in all the ROS assays were controlled within the same range by measuring its absorption of 450nm light with a U-3900H spectrophotometer (Hitachi, Japan). More specifically, the absorption levels measured by this equipment were always controlled in the range of 6.5-7. Then, the fungi were centrifuged and separated from the medium, and were dissolved in a 500-fold dilution of the ROS fluorescent probe (DCFH-DA assay kit, Beyotime Institute of Biotechnology, China) by phosphate buffer saline (PBS). After incubated at 37^oC in a shaker for half an hour, the suspension was centrifuged for three times to remove the redundant probe. Then, the suspension was seeded into a 96-well plate, and divided into a treatment group and a control group. The treatment group was irradiated respectively by the four LED light sources; while the control group was kept in the dark. Immediately after the light treatment, the intracellular ROS levels were measured as the fluorescent levels in a VL0L0TD0 Varioskan LUX microplate reader (Thermo Fisher, US), with the exciting and emitting wavelength respectively set at 488nm and 525nm. For each treatment interval, the plates were continuously exposed to the light, and were then discarded after the measurement by the microplate reader.

Triplicate experiments were performed in a similar fashion as described in the anti-fungal assays; i.e. respectively at the sampling instant of 0, 5, 10, 15, 20, 25 and 30 minutes under the 385nm, 405nm and 415nm light exposure; and at 0, 15, 30, 45, 60, 75, 90, 105 and 120 minutes under the 450nm light irradiation. The raw data were processed to produce the mean and standard deviation of the ROS fluorescent levels for each treatment time interval.

C. DYNAMIC MODEL OF ROS CONCENTRATIONS INDUCED BY PHOTON ENERGY

As introduced in Sec. I, although comprehensive models of the photosensitized oxidation reactions in PDTs have already been established in the literature, models of the induced ROS in vitro without utilizing any exogenous PS are not yet available. The difficulties can be attributed firstly to the many unknown parameters that must be determined from dedicated experiments, and secondly to the lack of knowledge about what types of reactions, endogenous PS and oxidants are exactly involved in anti-fungal therapies. To avoid these difficulties and reduce the experimental burdens, we propose to use a reduced model structure and estimate its parameters

from the ROS concentration data observed from experiments. The reduction from the highly coupled nonlinear Michaelis-Menten type models [13] does not take the short-time transient behaviour into account, and is only valid for modeling the ROS accumulations at a time scale larger than one minute. This is motivated by the fact that at a macroscopic time scale, the increasing trend of the singlet oxygen concentration [12] is similar to the step response of a first order linear dynamic system [17].

Denote the ROS concentration by y. The first order linear system description of its dynamics can be expressed by the following differential equation.

$$\frac{dy(t)}{dt} = -k \cdot y(t) + u, \tag{1}$$

where $t \geq 0$ is the time instant; $k > 0$ is the reaction rate constant; and $u > 0$ represents an unknown input, and is constant in the case of a step response. This model is actually an integrator, and is thus suitable to describe the accumulation of ROS over time. The solution of Eq. (1) takes an analytic form [17] as

$$\begin{aligned} y(t) &= e^{-kt} \cdot y_0 + \int_0^t u \cdot e^{-k(t-\tau)} d\tau, \\ &= \frac{u}{k} + \left(y_0 - \frac{u}{k}\right) \cdot e^{-kt}, \end{aligned}$$

where y_0 denotes the initial value of y at time instant 0. When $u > 0$ is constant for $t \geq 0$, this equation defines the step response of the dynamic system defined by Eq. (1). For brevity, the time variable will be omitted in what follows.

Equivalently, one can parameterize u as $u = k \cdot (y_0 + u')$, with $u' \geq 0$ arbitrary. Then, the above equation is further simplified to

$$y = y_0 + u' \cdot \left(1 - e^{-kt}\right).$$

Bringing y_0 to the left of the equal sign and dividing both sides by y_0, one can obtain the following equation of the relative change of the ROS concentration with respect to its initial value.

$$\underbrace{\frac{y - y_0}{y_0}}_{x} = \underbrace{\frac{u'}{y_0}}_{r} \cdot \left(1 - e^{-kt}\right). \tag{2}$$

For brevity, denote $\frac{y-y_0}{y_0}$ by x and $\frac{u'}{y_0}$ by r in what follows.

Note that since the ROS concentrations are actually measured with fluorescent probes, by e.g. a microplate reader, it is more meaningful to take the relative value x in Eq. (2). Besides, it is well known that ROS naturally exists in cells and regulates a great number of biochemical reactions, which generally accounts for 2% of the total oxygen consumed by mitochondria under a ''normal'' condition [23]. Therefore, an initial ROS concentration in the fungi always exists, and contributes to a nontrivial initial fluorescent level, i.e. $y_0 > 0$, before being irradiated by light.

Obviously, Eq. (2) is a monotonically increasing function of t. The only parameters of this model to be estimated are k and r. The formulation of Eq. (2) indicates that r can be interpreted as the ratio of the initial total concentration of the other molecules involved in the reactions (e.g. the triplet oxygen and all the three states of the endogenous PS) to the initial concentration of the ROS.

D. FUNCTIONAL RELATIONSHIP BETWEEN REACTION RATES AND PHOTON ENERGY

In classical PDT models, the PDT dose is defined as the number of photons absorbed by the PS, and is related to the irradiance and the photon energy [12], [24]. The kinetic PDT equations are henceforth parameterized by the irradiance and photon energy of the stimulating light.

The energy of a photon is inversely proportional to the wavelength of the light, which is usually given in the unit of electron-volt (eV, and $1eV = 1.602 \times 10^{-19}J$), i.e.

$$E_p = \frac{h \cdot c}{\lambda} = \frac{1.24}{\lambda}, \tag{3}$$

where h and c are respectively the Planck's constant and the speed of light. Here, the unit of λ shall be converted from nanometers to microns. Photon energy will also be used to quantify a specific light source in what follows.

For in vitro anti-fungal experiments, the photon energy is directly absorbed by fungal cells instead of tissues. On the other hand, according to the experimental results to be presented later in Sec. III, the reaction rate constants in Eq. (2) estimated from the experimental data using the four light spectra are all different, when keeping the light irradiance at the same level. More specifically, the rate constants at 415nm and 450nm are respectively the largest and the smallest; while those at 385nm and 405nm first show a ''roll-off'' after the rate peak near 415nm, and are then followed by an increasing

$$k = \begin{cases} a + b \cdot \sin(d \cdot E_p + \varphi), & E_p \leq \bar{E} \\ a + b \cdot \exp\left\{-[\alpha \cdot (E_p - \mu)]^c\right\} \cdot \sin(d \cdot E_p + \varphi), & E_p > \bar{E} \end{cases} \tag{4}$$

$$x(E_p, H_e) = \begin{cases} r \cdot \left\{1 - \exp\left\{-\frac{1}{E_e} \cdot \left[a + b \cdot \sin(d \cdot E_p + \varphi)\right] \cdot H_e\right\}\right\}, & E_p \leq \bar{E} \\ r \cdot \left\{1 - \exp\left\{-\frac{1}{E_e} \cdot \left\{a + b \cdot e^{-[\alpha \cdot (E_p - \mu)]^c} \cdot \sin(d \cdot E_p + \varphi)\right\} \cdot H_e\right\}\right\}, & E_p > \bar{E} \end{cases} \tag{5}$$

trend again (see Table 3 and Fig. 6). This pattern actually corresponds well to the more reported practices of using 400-420nm light in the anti-fungal experiments. Motivated by this observation, one can describe this dependence of the reaction rate constant on the photon energy by Eq. (4), as shown at the bottom of the previous page.

Here, $a, b, c, d, \alpha, \mu, \varphi$ are the parameters to be estimated; and $\bar{E}$ is the point at which the reaction rate starts to roll off. In the model (4), the sinusoidal function describes the peak near 415nm and the decreasing trend for longer wavelengths up to 460nm; while the exponentially decaying term, $\exp\left\{-[\alpha \cdot (E_p - \mu)]^c\right\}$, is to account for the roll-off after the rate peak.

E. MODELING ROS CONCENTRATION AS A FUNCTION OF PHOTON ENERGY AND FLUENCE

Now, by substituting Eq. (4) into Eq. (2) and noting that $t = H_e/E_e$, the model of the relative ROS concentration x as a function of the photon energy and fluence of the stimulating light can be finally derived, which takes $a, b, c, d, r, \alpha, \mu, \varphi$ and the light irradiance E_e as parameters. The model takes the form of Eq. (5), as shown at the bottom of the previous page.

F. MODELING FUNGAL VIABILITY AS A FUNCTION OF PHOTON ENERGY AND FLUENCE

Although a viability model is not required in the aforementioned ROS model, it is also relevant to further understand the effect of the photon energy and fluence on the efficiency of eliminating the fungi by the light. Such a mathematical relationship can be built in a similar fashion as in building the ROS model.

To this end, one first needs to fit a time-varying viability model of the fungi when being exposed to the light of each wavelength. Since it takes some time for the ROS concentration to reach a sufficient level to kill the fungi, a piecewise function including a "shoulder" [25] is suitable to describe such a process, i.e.

$$\rho(t) = \begin{cases} 1, & t \le \tau \\ e^{-k_v(t-\tau)}, & t > \tau \end{cases} \tag{6}$$

where $\rho(t)$ is the survival rate at time t; k_v is the decaying rate coefficient; and τ is the time constant when the inactivation starts.

The next step is also to fit the parameters k_v and τ to the photon energy, because they vary among the four different light wavelengths. Also according to the experimental results to be presented later in Sec. III, the models of k_v and τ are respectively parameterized as follows.

$$k_v = \exp\left(p_1 \cdot E_p^4 + p_2 \cdot E_p^3 + p_3 \cdot E_p^2 + p_4\right), \tag{7}$$

$$\tau = q_1 \cdot E_p^3 + q_2 \cdot E_p^2 + q_3 \cdot E_p + q_4. \tag{8}$$

Here, $p_i, q_i, i = 1, 2, 3, 4$ are the coefficients to be estimated. The exponential function in Eq. (7) is to enforce $k_v > 0$, since a pure polynomial function cannot ensure this, when k_v is close to zero.

Similarly, by substituting Eqs. (7, 8) into Eq. (6) and taking $t = H_e/E_e$, the model can be finally written as Eq. (9) as shown at the bottom of this page.

III. RESULTS

A. VIABILITY MEASUREMENTS OF C. ALBICANS

In the experiments with the 385nm, 405nm and 415nm light sources, no significant growth inhibition of *C. albicans* was observed until being irradiated for ten minutes ($p < 0.05$). After being exposed to the light for 25 or 30 minutes, the survival rates of the fungi all dropped below 20%. On the other hand, in the experiment with the 450nm light source, significant elimination of *C. albicans* was observed after being irradiated for 100 minutes ($p < 0.05$); while after two hours, about 80% of the fungi were inhibited. The viability rates of the four experiments are depicted in Fig. 2. As an illustrative example, the fungal growth on the agar plates after being irradiated by the 385nm light for different durations from 0 to 30 minutes is shown in Fig. 2(e). The decreasing trend of the CFU can be clearly observed.

B. ROS MEASUREMENTS

The time sequences of the measured ROS concentrations in the *C. albicans* were measured from the experiments using all the four different light sources. The measured fluorescent levels y were processed according to the definition of Eq. (2) as $x = \frac{y-y_0}{y_0}$, where y_0 is the initial level. The relative changes in the ROS concentrations due to the light stimulation are plotted in Fig. 3.

To visualize the gradual accumulations of the ROS in the fungi as the light exposure continues, the time-lapse images of the fungal cells after being irradiated by the 405nm light for different durations from 0 to 30 minutes were taken by an Axio Observer A1 inverted fluorescence microscope (ZEISS, Germany), and are illustrated in Fig. 3(e). The exciting and emitting wavelength were set respectively at 488nm and 525nm. The increasing trend of the ROS concentrations can be clearly observed.

$$\rho(E_p, H_e) = \begin{cases} 1, & H_e \le E_e \cdot \sum_{i=1}^{4} q_i \cdot E_p^{4-i} \\ \exp\left\{-\exp\left(\sum_{i=1}^{3} p_i \cdot E_p^{5-i} + p_4\right) \cdot \left(\frac{H_e}{E_e} - \sum_{i=1}^{4} q_i \cdot E_p^{4-i}\right)\right\}, & \text{otherwise.} \end{cases} \tag{9}$$

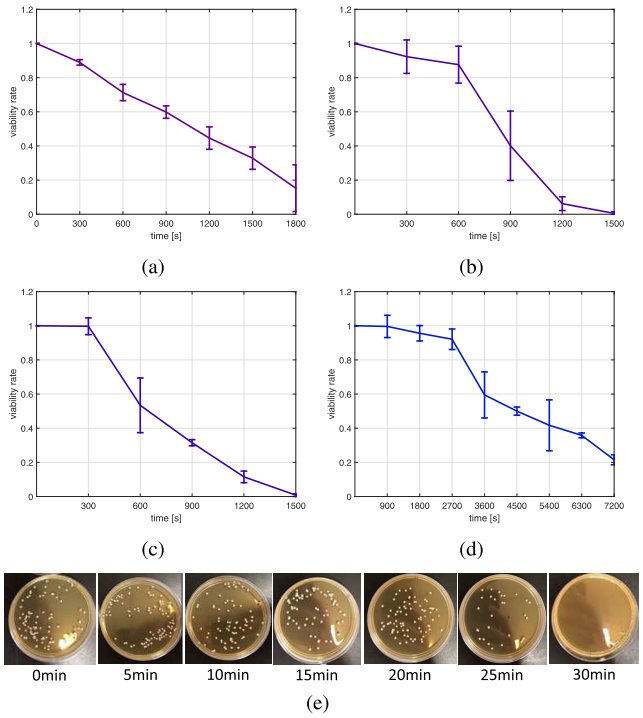

FIGURE 2. Measured viability rates of the *C. albicans* irradiated respectively by (a) 385nm, (b) 405nm, (c) 415nm, (d) 450nm LED light source, and (e) the pictures of the fungal growth on the agar plates after being irradiated by the 385nm light for different durations from 0 to 30 minutes.

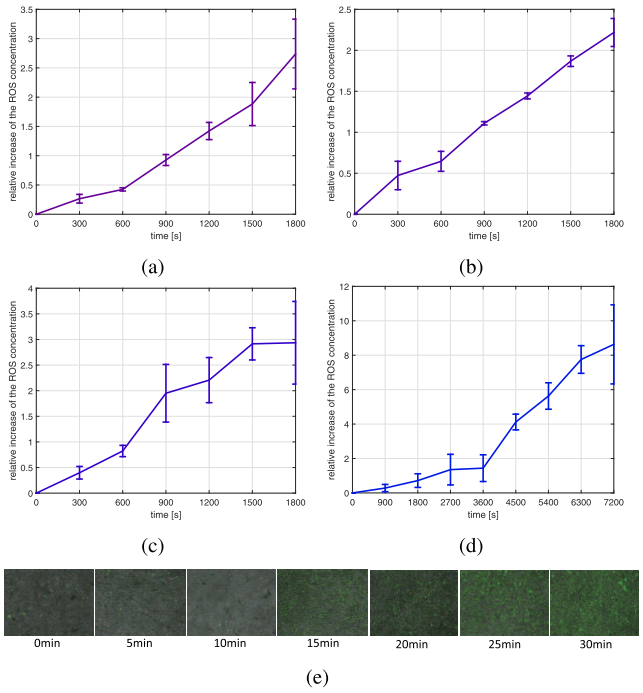

FIGURE 3. Measured relative changes in the ROS fluorescent levels in the *C. albicans* irradiated respectively by (a) 385nm, (b) 405nm, (c) 415nm, (d) 450nm LED light source, and (e) the time-lapse ROS fluorescent images of the fungal cells taken from 0 to 30 minutes with a 5min time difference.

C. ESTIMATION OF THE PARAMETERS OF EQ. (2)

Eq. (2) contains two parameters to be estimated, i.e. r and k. By definition, this estimation problem is nonlinear, and can be solved by a standard nonlinear least-squares (NLS) algorithm [26], e.g. the Levenberg-Marquardt method. The dependence of the RMSE fitting errors on the values of r and k is shown in Fig. 4. It can be seen that in all the four cases, the optimum of the parameter pair (r, k) lies on the flat bottom of a narrow valley roughly within the range of $30 \leq r \leq 3000$ and $10^{-4} \leq k \leq 10^{-6}$. The gradients of the fitting errors with respect to this pair are approximately zero within this valley. In other words, the NLS optimization is likely to terminate at any point in this valley depending on the specified initial values and stopping conditions, which can also been seen from Fig. 4. Based on this observation, it is better to fix r to a value in the range of $30 \leq r \leq 3000$, and estimate k by linear least-squares (LS), which is guaranteed to result in a unique global optimal solution. Moreover, it is also necessary to set r to a same value, in order to compare the effects of the four wavelengths on the reaction rates k.

On the other hand, note that the fungi used in this work are of the same type, and were cultivated and processed following exactly the same protocols. It is hence also reasonable to assume that the parameter r in all the experiments is of the same value. According to the interpretation of r in Eq. (2), this physically means that the ratios of the initial total concentration of the other molecules involved in the reactions (e.g. the triplet oxygen and all the three states of the

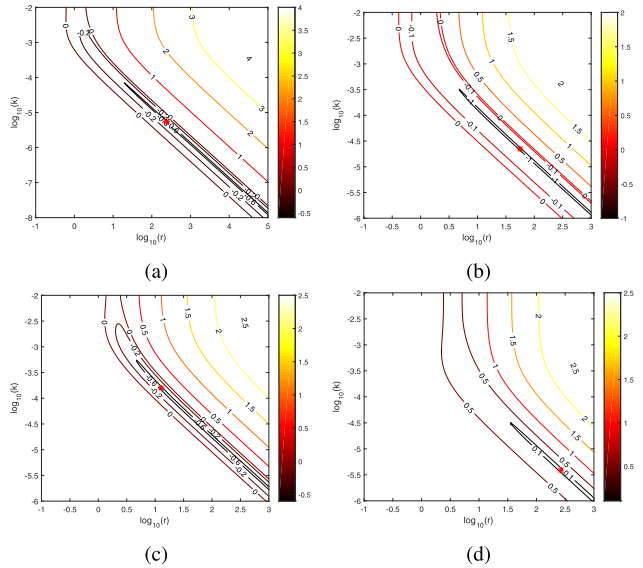

FIGURE 4. Dependence of the RMSE fitting errors on the values of r and k: (a) 385nm, (b) 405nm, (c) 415nm, (d) 450nm. Contours: $\log_{10}(RMSE)$; Stars: the NLS estimates.

endogenous PS) to the initial ROS concentration can be assumed to be at the same level in all the experiments. When there is an ample amount of oxygen molecules in the cells, i.e. when r is dominated by the ratio between the concentration of the initial triplet oxygen and the initial ROS, one can take $r = 50$, since in the normal condition of mitochondrial respiration, ROS takes about 2% of the total oxygen

TABLE 3. Estimated reaction rate constants and RMSE fitting errors.

	k	$RMSE$
385nm	2.65E-5	0.240
405nm	2.50E-5	0.056
415nm	3.68E-5	0.216
450nm	2.22E-5	1.233

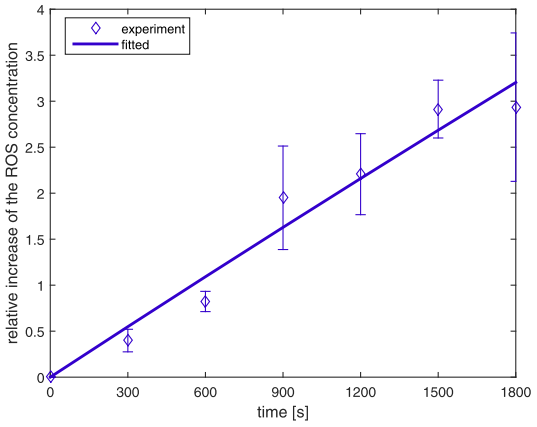

FIGURE 5. Fitted curve to the measured relative ROS concentration data from the 415nm light irradiation experiment.

consumption [23]. More specifically, by fixing r, k can be estimated by solving the following LS problem.

$$k \cdot t = -\ln\left(1 - \frac{x}{r}\right). \tag{10}$$

The LS estimates and the RMSE fitting errors are listed in Table 3. As an illustrative example, the model fitted to the data from the 415nm light irradiation experiment is depicted in Fig. 5.

D. ESTIMATION OF THE PARAMETERS OF EQ. (4)

The estimated reaction rate constants in Table 3 and their corresponding photon energy in Table 2 are plotted in Fig. 6. Note that in Eq. (4), there are totally seven unknown parameters to be estimated, i.e. $a, b, c, d, \alpha, \mu, \varphi$. However, there are only four data points, which can at most uniquely determine four parameters. To solve them, d was first determined by estimating the period of the sinusoidal function from the four target points, by noting that the range of the photon energy shall be within one complete period of the sinusoidal function (otherwise, there will be multiple peaks). On the other hand, $\bar{E}$ that determines the roll-off point shall be between 2.98 and 3.09; and α, μ are intended to shift and normalize the photo energy into the range between 0 and 1. This then reduces the number of unknown parameters to three, which can be solved by a standard NLS algorithm. The finally estimated parameters are listed in Table 4, which perfectly fits to the four target points with an RMSE fitting error of 7.86E-7.

E. SIMULATING THE ROS MODEL WITH VARIOUS PHOTON ENERGY AND FLUENCE

With the parameters in Table 4 and taking $r = 50$ and $E_e = 50mW/cm^2$, the model of the ROS concentration as a function of the stimulating photon energy and fluence,

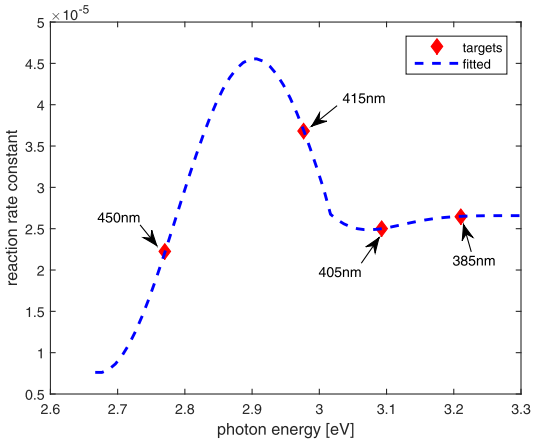

FIGURE 6. Fitted model of the reaction rate constants as a function of the photon energy. The arrows indicate the experimenting light sources. The simulated range of the photon energy $2.7 \sim 3.3eV$ corresponds to the wavelength range of $375 \sim 460nm$.

TABLE 4. Estimated parameters of Eq. (4).

a	b	c	d	α	μ	φ	$\bar{E}$
2.66E-5	1.90E-5	3.025	13.57	3.100	2.667	-31.55	3.012

i.e. Eq. (5), was finally simulated. The results are plotted in Fig. 7.

F. SUMMARY OF THE PROCEDURES TO BUILD THE ROS MODEL

Although a single strain of *C. albicans* was tested in this work, the proposed modeling method can actually be applied to other fungal species, as well. The experimental and modeling procedures follow the steps shown in Fig. 8.

G. FITTING AND SIMULATION OF THE VIABILITY MODEL

Since the main purpose of this work is to build the ROS model, and also for brevity, the detailed parameter estimation procedures for the viability model will be omitted; and only the fitting results are presented here.

The parameters k_v and τ were first fitted to the viability data as shown in Fig. 2, whose estimated values for all the four wavelengths are listed in Table 5. The estimated coefficients of the polynomials in Eqs. (7, 8) are listed in Table 6, which resulted in the fitted curves as illustrated in Fig. 9. With these estimated parameters, the viability model was finally simulated. The results are plotted in Fig. 10.

IV. DISCUSSION

In this study, anti-fungal light irradiation experiments were conducted using four different wavelengths, in which both the viability of the fungi and the generated ROS therein were measured. The main objectives are to compare the effects of four different wavelengths in terms of their effect in inducing ROS, and to build a mathematical model that relates the ROS generation with the photon energy and the fluence of the stimulating light.

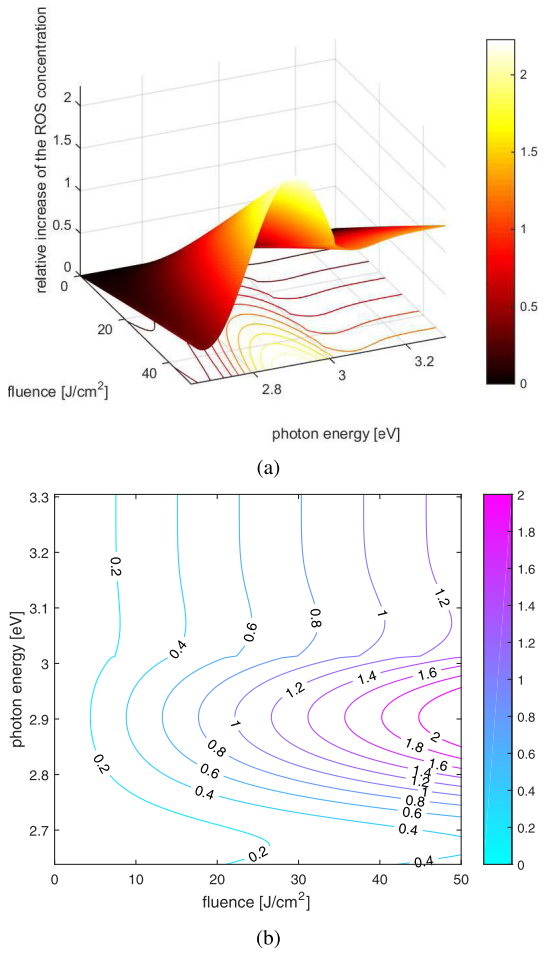

FIGURE 7. Relative increase of the ROS concentration in response to various photon energy and fluence: (a) 3D plot, (b) contour plot.

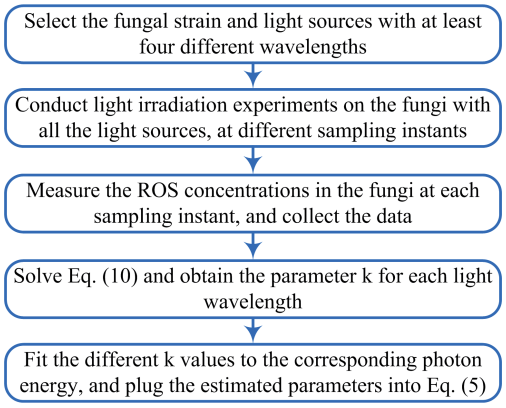

FIGURE 8. Procedures of implementing the data-driven modeling method.

TABLE 5. Estimated parameters of Eq. (6).

	k_v	τ *(in sec.)*	*RMSE*
385nm	1E-3	226.80	0.235
405nm	7.06E-3	770.70	0.056
415nm	3.85E-3	447.30	0.211
450nm	2.89E-4	2232.72	1.176

The viability data in Fig. 2 show that the 415nm light performed best in eliminating *C. albicans* in terms of the lowest survival rate of the fungi after having been irradiated for 25 minutes. The longest wavelength 450nm turned out to be the worst in this aspect, because of the much longer time it took to significantly kill the fungi. On the other hand, a "shoulder" in the viability curve of the fungi can be clearly seen in most cases. The shoulders indicate that the fungi were not immediately killed right after being exposed to the light. This can be attributed to the fact that the main hypothesized mechanism of anti-fungal light therapies is the cytotoxicity due to the induced ROS from the interaction between the light and the endogenous PS. To generate enough toxicity to kill the fungi, the ROS in the cells needs to accumulate to a sufficient level. The turning point appeared when all the four wavelengths led to more than 40% fungal elimination. These points were respectively at 900sec for 385nm and 405nm, at 600sec for 415nm, and at 3600sec for 450nm. At these points, the relative ROS increases were of similar values around 1, i.e. 1.11±0.02, 0.93±0.09, 0.82±0.11, 1.44±0.78 respectively for the 385nm, 405nm, 415nm and 450nm light.

TABLE 6. Estimated coefficients of the polynomials in Eqs. (7, 8).

	p_1 or q_1	p_2 or q_2	p_3 or q_3	p_4 or q_4	*RMSE*
Eq. (7)	-37.23	287.19	-620.59	841.56	9.20E-16
Eq. (8)	-1.53E5	1.39E6	-4.19E6	4.22E6	2.38E-9

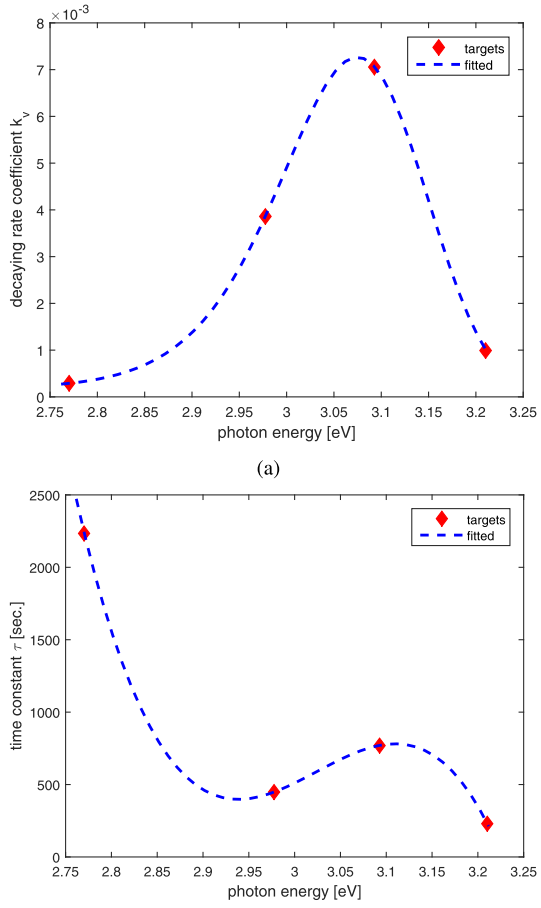

FIGURE 9. Fitted model of k_V and τ as a function of the photon energy: (a) k_V as in Eq. (7), (b) τ as in Eq. (8).

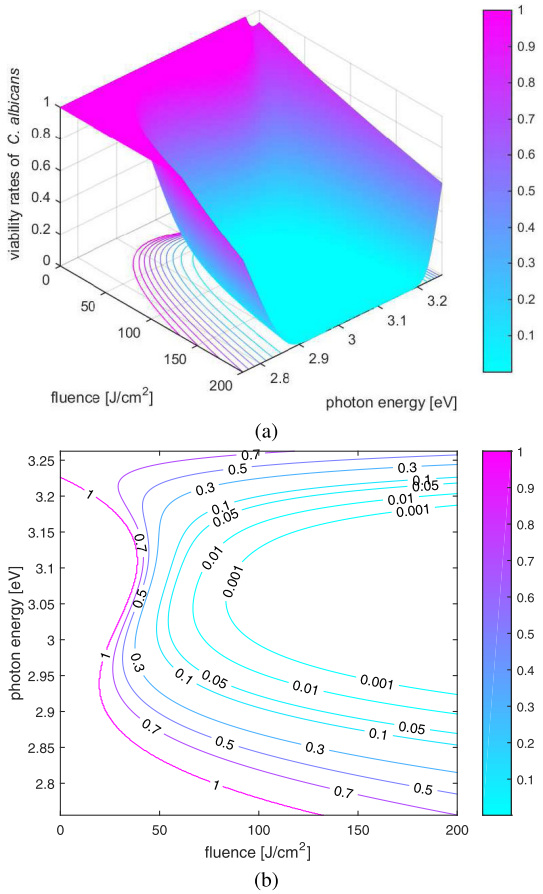

FIGURE 10. Variation of the fungal viability rates in response to various photon energy and fluence: (a) 3D plot, (b) contour plot.

On the other hand, in the case of the 385nm-light irradiation, the fungi appeared to start degenerating sooner than the cases of using the 405nm and 415nm light. This indicates that the UVA light of 385nm may cause other more dramatic inhibiting effects to the fungi besides inducing ROS, e.g. causing tryptophan photodegradation within the cells [27]. Moreover, as can be observed from the simulated fungal viability rates in response to various photon energy and fluence as in Fig. 10, the most effective anti-fungal photon energy is in the range of 2.85∼3.2eV, corresponding to wavelength range of 387.5∼435nm.

Due to the aforementioned challenges to parameterize the model of the induced ROS concentrations in vitro without utilizing any exogenous PS, a data-driven modeling approach was proposed. This modeling approach mainly takes into account the long time scale ROS accumulating effect during light irradiation. The analysis of the dependence of the RMSE fitting errors on the values of the two model parameters, i.e. r and k, show that their optimal values are actually trapped within a flat and narrow valley. In this valley, the gradients of the cost function with respect to these two parameters are almost trivial. Therefore, instead of leaving the optimization to stop at a random point in this valley (depending on the randomly given initial value and stopping criteria), the value of r was fixed to 50. Consequently, the reaction rate constant k can be estimated as a linear LS problem, which ensures that the unique global optimal value of k can be found. Here, a mild assumption is made that r is dominated by the ratio between the concentrations of the initial triplet oxygen and the initial ROS. Therefore, its value can be taken as 50, due to the aforementioned fact that in the normal condition of mitochondrial respiration, ROS takes about 2% of the total oxygen consumption. Good agreement of the fitted functions with the experimental data was achieved for the four data sets, as shown in Table 3 and Fig. 5. This demonstrates the validity of the proposed model structure and the assumption.

The estimated reaction rate constants show a dependence on the wavelengths or their corresponding photon energy, which peak near 415nm and decline to the minimum as the wavelength increases to 460nm. According to Eq. (2), the reaction rate constant determines the speed of generating ROS in the photochemical reaction. The larger the value, the faster the accumulation of the cytotoxic ROS, and thus the faster the elimination of the fungi. On the other hand, the roll-off effect of the reaction rate at even shorter wavelengths, i.e. 385nm and 405nm, indicates that the sensitivity of the endogenous PS to UVA light is lower than that to the light in the range of 415∼426nm. However, the similar anti-fungal effect of 385nm and 405nm with that of 415nm indicate that other inhibiting effects to the fungi besides inducing ROS might have also been induced by these wavelengths, e.g. causing tryptophan photodegradation [27].

It is known in the literature that there are several types of endogenous PS responsible for anti-fungal effects, including various kinds of porphyrins and flavins, depending on the fungal species. The Soret bands of porphyrins are generally in the range of 400∼410nm [28]; while some types can reach 413∼416nm [29]. On the other hand, the Soret bands of flavins are usually at longer wavelengths. For instance, the peak absorption of acriflavin neutral (or euflavine) is at 436nm [30]; and that of cytochrome-flavin complex is at 427nm [31]. In fact, the fitted model of Eq. (4) reveals that in the experiments the peak absorption wavelength is at 426.6nm or 2.907eV in photon energy. This indicates that there may be more than one type of endogenous PS in the $C.\ albicans$ studied in this work, which all contribute to the generation of ROS.

By simulating the model of the ROS concentration as a function of the photon energy and fluence, the following observations can be further made. First, when the fluence is small, i.e. $H_e < 5J/cm^2$, the induced ROS concentration is not much for any photon energy in the range of 2.7∼3.3eV. This indicates that the radiometric energy of the stimulating light needs to be higher than a threshold to trigger sufficient ROS generation, no matter how large the photon energy is. Second, as the fluence accumulates to a certain level, i.e. $H_e > 10J/cm^2$, the effects of the photon energy start to manifest. For this studied fungal strain, the range of photon energy 2.85∼2.95eV (or 420∼435nm in wavelength) demonstrated a higher efficiency in generating ROS.

These observations can be helpful to design the therapeutic devices and the doses used in treating the infections caused by this type of fungi.

On the other hand, the proposed model in this work also has some limitations. First, the proposed model structure is simplified, and cannot describe the transient dynamics of the PS and ROS. As another limitation, the proposed model does not distinguish different types of ROS. As being fitted to the general oxidative stress measured by the standard ROS assay kit, the output of the model is the changing rate of the total ROS accumulation, and hence contains the contributions from all the existing PS in the fungi.

V. CONCLUSION

In this work, a modeling approach has been developed to mathematically describe the induced ROS in fungi, as a function of the photon energy and fluence of the stimulating light. The method of estimating the model parameters from experimental data has also been proposed and verified. The fitting results agree well with the main trends of the experimental data at long time scales, e.g. from tens of minutes to a few hours. This indicates that the proposed model structures and the parameter estimation methods are effective to calculate the amount of accumulating ROS in the *C. albicans*, when being stimulated by the photon energy in the range of $2.7 \sim 3.3eV$.

As another main conclusion, the photon energy within the range of 2.85∼2.95eV (or 420∼435nm in wavelength) is more effective in generating ROS in the fungi studied in this work, and is hence more effective in treating the infections caused by this type of fungi.

As a potential future extension, the data-driven modeling approach can be further extended to account for the individual contributions of the main types of endogenous PS in the fungi to the generation of ROS. Another extension will be to develop a data-driven approach to model the in vivo ROS generation.

REFERENCES

[1] R. A. Calderone and W. A. Fonzi, "Virulence factors of Candida albicans," *Trends Microbiol.*, vol. 9, no. 7, pp. 327–335, Jul. 2001.

[2] T. Arendorf and D. Walker, "The prevalence and intra-oral distribution of Candida albicans in man," *Arch. Oral Biol.*, vol. 25, no. 1, pp. 1–10, 1980.

[3] J. D. Sobel, "Vaginitis," *New England J. Med.*, vol. 337, no. 26, pp. 1896–1903, 1997.

[4] A. Erdogan and S. S. C. Rao, "Small intestinal fungal overgrowth," *Current Gastroenterol. Rep.*, vol. 17, no. 4, 2015, Art. no. 16.

[5] T. Maisch, "A new strategy to destroy antibiotic resistant microorganisms: Antimicrobial photodynamic treatment," *Mini-Rev. Med. Chem.*, vol. 9, no. 8, pp. 974–983, Jul. 2009.

[6] R. Yin, T. Dai, P. Avci, A. E. S. Jorge, W. C. De Melo, D. Vecchio, Y.-Y. Huang, A. Gupta, and M. R. Hamblin, "Light based anti-infectives: Ultraviolet C irradiation, photodynamic therapy, blue light, and beyond," *Current Opinion Pharmacol.*, vol. 13, no. 5, pp. 731–762, Oct. 2013.

[7] W. J. Trzaska, H. E. Wrigley, J. E. Thwaite, and R. C. May, "Species-specific antifungal activity of blue light," *Sci. Rep.*, vol. 7, no. 1, p. 4605, 2017.

[8] Y. Zhang, Y. Zhu, J. Chen, Y. Wang, M. E. Sherwood, C. K. Murray, M. S. Vrahas, D. C. Hooper, M. R. Hamblin, and T. Dai, "Antimicrobial blue light inactivation of candida albicans: *In vitro and in vivo* studies," *Virulence*, vol. 7, no. 5, pp. 536–545, 2016.

[9] M. S. Baptista, J. Cadet, P. Di Mascio, A. A. Ghogare, A. Greer, M. R. Hamblin, C. Lorente, S. C. Nunez, M. S. Ribeiro, A. H. Thomas, M. Vignoni, and T. M. Yoshimura, "Type I and type II photosensitized oxidation reactions: Guidelines and mechanistic pathways," *Photochem. Photobiol.*, vol. 93, no. 4, pp. 912–919, Jul. 2017.

[10] X. Wang, Y. Liu, Z. Tan, and L. Chang, "Effects of oxygen concentration on the reactive oxygen species density under different operating conditions in atmospheric-pressure helium/oxygen pulsed dielectric barrier discharge," *IEEE Access*, vol. 7, pp. 69748–69757, 2019.

[11] K. Kang-Hsin Wang, S. Mitra, and T. H. Foster, "A comprehensive mathematical model of microscopic dose deposition in photodynamic therapy," *Med. Phys.*, vol. 34, no. 1, pp. 282–293, Dec. 2006.

[12] T. C. Zhu, J. C. Finlay, X. Zhou, and J. Li, "Macroscopic modeling of the singlet oxygen production during PDT," *Proc. SPIE*, vol. 6427, Mar. 2007, Art. no. 642708.

[13] M. M. Kim, A. A. Ghogare, A. Greer, and T. C. Zhu, "On the *in vivo* photochemical rate parameters for PDT reactive oxygen species modeling," *Phys. Med. Biol.*, vol. 62, no. 5, pp. R1–R48, Mar. 2017.

[14] K. A. Johnson and R. S. Goody, "The original Michaelis constant: Translation of the 1913 Michaelis–Menten paper," *Biochemistry*, vol. 50, no. 39, pp. 8264–8269, Oct. 2011.

[15] G. Kareliotis, S. Liossi, and M. Makropoulou, "Assessment of singlet oxygen dosimetry concepts in photodynamic therapy through computational modeling," *Photodiagnosis Photodyn. Therapy*, vol. 21, pp. 224–233, Mar. 2018.

[16] K. W. Beeson, E. Parilov, M. Potasek, M. M. Kim, and T. C. Zhu, "Validation of combined Monte Carlo and photokinetic simulations for the outcome correlation analysis of benzoporphyrin derivative-mediated photodynamic therapy on mice," *J. Biomed. Opt.*, vol. 24, no. 3, p. 1, Mar. 2019.

[17] K. Åström and B. Wittenmark, *Computer-Controlled Systems: Theory and Design*. Upper Saddle River, NJ, USA: Prentice-Hall, 1984.

[18] J. Zhang, D. Xing, and X. Gao, "Low-power laser irradiation activates Src tyrosine kinase through reactive oxygen species-mediated signaling pathway," *J. Cell. Physiol.*, vol. 217, no. 2, pp. 518–528, Nov. 2008.

[19] A. Lynnyk, M. Lunova, M. Jirsa, D. Egorova, A. Kulikov, Š. Kubinová, O. Lunov, and A. Dejneka, "Manipulating the mitochondria activity in human hepatic cell line Huh7 by low-power laser irradiation," *Biomed. Opt. Express*, vol. 9, no. 3, p. 1283, Mar. 2018.

[20] J. Dong and Z. Zhang, "Design of LED light for stimulating cells in the study of light therapies," in *Proc. 15th SSLChina, IFWS*, Oct. 2018, pp. 74–77.

[21] J. Dong and D. Xiong, "Applications of light emitting diodes in health care," *Ann. Biomed. Eng.*, vol. 45, no. 11, pp. 2509–2523, 2017.

[22] J. Dong and G. Zhang, "Identification and robust control of the nonlinear photoelectrothermal dynamics of LED systems," *IEEE Trans. Ind. Electron.*, vol. 64, no. 3, pp. 2215–2225, Mar. 2017.

[23] D. B. Zorov, M. Juhaszova, and S. J. Sollott, "Mitochondrial reactive oxygen species (ROS) and ROS-induced ROS release," *Physiolog. Rev.*, vol. 94, no. 3, pp. 909–950, Jul. 2014.

[24] F. Cieplik, A. Pummer, J. Regensburger, K. Hiller, A. Späth, L. Tabenski, W. Buchalla, and T. Maisch, "The impact of absorbed photons on antimicrobial photodynamic efficacy," *Frontiers Microbiol.*, vol. 6, p. 706, Jul. 2015.

[25] R. L. Buchanan, M. H. Golden, and R. C. Whiting, "Differentiation of the effects of pH and lactic or acetic acid concentration on the kinetics of listeria monocytogenes inactivation," *J. Food Protection*, vol. 56, no. 6, pp. 474–478, Jun. 1993.

[26] P. Hansen, V. Pereyra, and G. Scherer, *Least Squares Data Fitting with Applications*. Baltimore, ML, USA: Johns Hopkins Univ. Press, 2012.

[27] M. R. Hamblin, "Mechanisms and mitochondrial redox signaling in photobiomodulation," *Photochem. Photobiol.*, vol. 94, no. 2, pp. 199–212, Mar. 2018.

[28] A. Del C. Batlle, "Porphyrins, porphyrias, cancer and photodynamic therapy—A model for carcinogenesis," *J. Photochem. Photobiol. B, Biol.*, vol. 20, no. 1, pp. 5–22, Sep. 1993.

[29] R. Sampaio, M. Silva, A. Batista, and N. Neto, "Investigation of the photophysical and eletrochemical properties of a free base tetrapyridyl porphyrin with meso carbon linked ruthenium(II) groups," *J. Photochem. Photobiol. A, Chem.*, vol. 315, pp. 98–106, Jan. 2016.

[30] L. Y. Brovko, A. Meyer, A. S. Tiwana, W. Chen, H. Liu, C. D. M. Filipe, and M. W. Griffiths, "Photodynamic treatment: A novel method for sanitation of food handling and food processing surfaces," *J. Food Protection*, vol. 72, no. 5, pp. 1020–1024, May 2009.

[31] T.-Y. Leong, R. D. Vierstra, and W. R. Briggs, "A blue light-sensitive cytochrome-flavin complex from corn coleoptiles. Further characterization," *Photochem. Photobiol.*, vol. 34, no. 6, pp. 697–703, Dec. 1981.

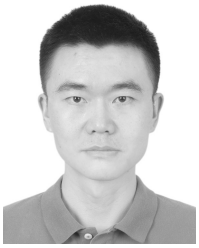

JIANFEI DONG received the M.Eng. degree from the National University of Singapore, Singapore, in 2005, and the Ph.D. degree in systems and control from the Delft University of Technology (TUD), Delft, The Netherlands, in 2009.

From November 2009 to July 2011, he was a Postdoctoral Researcher with TUD. Then, he worked as a Research Scientist with Philips Research, Eindhoven, The Netherlands. He is currently a Professor with the Suzhou Institute of Biomedical Engineering and Technology, Chinese Academy of Sciences, Suzhou, China. His current research interests include data-driven modeling and control methodologies for complex dynamic systems, including biological, optoelectronic and mechatronic systems, and development of optical devices for diagnosis and therapies.

TIANFENG WANG received the B.Eng. degree from the University of Science and Technology of China, in 2015, and the M.Eng. degree from The State University of New York at Buffalo, in 2017. He is currently pursuing the Ph.D. degree with the Suzhou Institute of Biomedical Engineering and Technology, Chinese Academy of Sciences, Suzhou, China, and also with the Delft University of Technology, Delft, The Netherlands. His main research area is mechanism of light therapies.